Optik - International Journal for Light and Electron Optics 273 (2023) 170455

Contents lists available at ScienceDirect

Optik

journal homepage: www.elsevier.com/locate/ijleo

Original research article

On the optical constants of cobalt in the M-absorption edge region

Qais Saadeh [a,*], Philipp Naujok [b], Devesh Thakare [c], Meiyi Wu [c], Vicky Philipsen [c], Frank Scholze [a], Christian Buchholz [a], Zanyar Salami [a], Yasser Abdulhadi [a], Danilo Ocaña García [a], Heiko Mentzel [a], Anja Babuschkin [a], Christian Laubis [a], Victor Soltwisch [a]

[a] Physikalisch-Technische Bundesanstalt (PTB), Abbestraße 2-12, 10587 Berlin, Germany
[b] OptiX fab GmbH, Otto-Schott-Str. 41, 07745 Jena, Germany
[c] Imec, Kapeldreef 75, B-3001 Leuven, Belgium

ARTICLE INFO

Keywords:
Cobalt
Carbon
Optical constants
Extreme ultraviolet
Thin films
X-ray reflectivity

ABSTRACT

Using monochromatized synchrotron radiation, the optical constants of cobalt are determined in the spectral range 8.0–25.0 nm. The optical constants are determined from Angle-Dependent Reflectometry (ADR) measurements of a multilayer sample. Since cobalt is prone to strong oxidation, carbon capping was used to stabilize the probed sample. The fine-structure of the optical constants in the M-absorption edge region is resolved with unprecedented resolution for the element. The determination of the optical constants from reflectivity data was conducted using Markov Chain Monte Carlo (MCMC) based Bayesian inferences, supported with X-ray Reflectivity (XRR) data. This work further demonstrates establishing MCMC-based Bayesian inferences for determining optical constants. Time-Frequency Analysis (TFA) methods are also used to solve the corresponding inverse problem by supporting initializing a model of the sample. The results here are highly relevant for developing Co-based Multilayer Mirrors (MLMs) targeting the Extreme Ultraviolet (EUV) range, particularly those MLMs dedicated for EUV astronomy.

1. Introduction

Extreme Ultraviolet Lithography (EUVL) systems are coping with High-Volume Manufacturing (HVM) requirements and their importance is increasing significantly. Research is ongoing to assist mitigating the inherent challenges in utilizing Extreme Ultraviolet (EUV) radiation for photolithography. Another priority is to further develop the current EUVL technology to achieve a greater node-feature miniaturization for semiconductor devices. In a lithography system, higher resolution can be achieved using a higher Numerical Aperture (NA), realizing that for EUVL requires improvements on the currently available optical elements. A system with a NA of 0.55 is a major improvement over the currently deployed EUVL scanners with a NA of 0.33 [1,2]. Generally, an obstacle for the development of optical elements for EUV-based technologies is that optical constants of many materials are poorly determined. The lack of accurate optical constants complicates the proper material selection, which precedes the design of any optical system.

In addition to lithography, EUV radiation is used for numerous applications, including spectroscopy [3], astronomy [4], scatterometry and imaging [5–7]. In this study, we report the determination of cobalt's optical constants in the spectral range 8.0–25.0 nm (ca. 49.6 eV–ca. 155 eV) from Angle-Dependent Reflectometry (ADR) measurements of a multilayer sample. The measurements were

* Corresponding author.
E-mail address: qais.saadeh@ptb.de (Q. Saadeh).

https://doi.org/10.1016/j.ijleo.2022.170455
Received 1 July 2022; Received in revised form 29 November 2022; Accepted 18 December 2022
Available online 19 December 2022

performed in the radiometry laboratory of the Physikalisch-Technische Bundesanstalt (PTB), in the electron storage ring BESSY II of the research institute Helmholtz-Zentrum Berlin (HZB). A by-product of this investigation is a review of the available optical data of C in the EUV spectral range, since a C capping layer was used to prevent the oxidation of Co.

The optical constants are commonly expressed as functions of the wavelength via the complex index of refraction $\overline{n}$; $\overline{n}(\lambda) = 1-\delta(\lambda) + i\beta(\lambda)$. $1-\delta(\lambda)$ (refractive index) and $\beta(\lambda)$ (extinction coefficient) indicate the phase velocity and the absorption of an electromagnetic radiation with a wavelength λ, respectively. In the EUV range, optical constants are usually determined either with ADR or from Transmission-Mode Measurements (TMM) [8,9]. ADR is used here since it allows the simultaneous determination of the two components of $\overline{n}$. TMM can yield the extinction coefficient directly, but requires optical data traversing the electromagnetic spectrum to properly enable calculating the real part of $\overline{n}$. A detailed discussion on optical constants and their determination methods can be found in refs [9–11].

The optical constants of cobalt have been reported before [12–14]. However, inconsistencies are observed between our results and the tabulated values of Henke et al. [12], Palik and those predicted by Chantler [13,14].

Cobalt thin films are used for a variety of applications. Spintronics and Giant Magnetoresistance (GMR) devices are two examples [15]. In the EUV, Co has been widely used in the coatings of optical elements. In 1993, a Co-based Multilayer Mirror (MLM) for a telescope targeting a wavelength of 6.35 nm was characterized in the radiometry laboratory of the PTB [16]. Regarding other research groups, Co/Mg and Co/Mg/B_4C MLMs have been investigated for their applicability in the EUV range, with Co/Mg showing encouraging results in the vicinity of the wavelength of 25 nm [17,18]. As well in the vicinity of a wavelength of 25 nm, a trilayer system of cobalt, magnesium and zirconium has demonstrated relatively highly reflectivity and thermally stable performance [19]. Generally, Co based MLMs have been extensively investigated for their anticipated thermal stability, given cobalt's relatively high melting temperature and other traits [19]. The spectral characteristics of Co/C MLMs were also reported in the vicinity of a wavelength of 7.5 nm [20]. Some MLMs incorporating Co coatings were reported to have "good performance" for the wavelength range 5.0–10.0 nm [21]. In addition, Co/Mg MLMs have been reported to exhibit relatively high reflectivity in the wavelength range 1.77–3.1 nm [22].

For EUVL and of our work in particular, initially, elemental Co has been investigated for its ability to serve as an alternative for the used tantalum-based photomask's absorber layer. Given its relatively high extinction coefficient, it could partially mitigate the so-called *photomask 3D effects* [23,24]. For the same, purpose we have also investigated binary alloys of tantalum and cobalt [25].

We further emphasize the applicability of Markov Chain Monte Carlo (MCMC) based Bayesian inferences for the determination of optical constants from EUV Reflectivity (EUVR) data. The problem focuses on resolving the fine-structure in the optical constants over a highly-technologically relevant spectral range, where determining the optical constants is particularly challenging. Given that the optical constants are determined using ADR via an inverse-problem, although the initialized parameters' prior range is enormous in our case, yet, plausible results are obtained. The method of MCMC-based Bayesian inferences is demonstrated to overcome poorly defined initialization constraints, albeit at the cost of the computational effort.

Co is prone to oxidation and it reacts with Si, which is the most used substrate material in the semiconductor industry. To prevent oxidation and interdiffusion, a multilayer thin film sample where elemental Co is sputtered on a Ru-underlayer and capped with C has been fabricated. The presence of such additional layers is necessary but brings issues for the corresponding inverse-problem because of the large number of added optimization parameters. The additional parameters in the inverse-problem make a straightforward approach impractical, i.e., leaving all the relevant parameters of the additional layers free. Therefore, parameterization of C optical constants at longer wavelengths using exponential-functions is presented as an approach to significantly reduce the number of free parameters.

With a concise discussion on the determination of optical constants from reactive materials, this work is also relevant to solid-state physics. The resolved fine-structure in the M-absorption edge region provides an insight for the predicted 3p subshells transitions splitting [26]. The increasing availability of EUV lab-sources facilitated studies of transition metals resonances at the M-edge, that is particularly interesting for having better understanding of magneto-optical effects like the magneto-optical Kerr effect and Magnetic Circular Dichroism (MCD) [27,28], but such studies are challenged sometimes due to the limited experimental optical data in the EUV range. Our results would further facilitate the understanding the magneto-optical effects observed for Co where the optical constants are involved.

2. Experimental setups

2.1. Coating process

Two samples were fabricated. A (bare) cobalt thin film with a nominal thickness of 30 nm and another multilayer where a Co thin film with a nominal thickness of 40 nm is *sandwiched* between C capping and a Ru underlayer. The samples were coated using Direct Current (DC) magnetron sputtering onto super-polished 300 mm Si wafers. After evacuating the chamber ($p_0 < 10^{-7}$ mbar) of the sputtering system, highly pure Ar gas (6N) was purged as a sputtering gas (sputtering pressure $p = 10^{-3}$ mbar). The native oxides of the substrates were not etched prior to deposition. Finally, the coated wafers were cut into smaller square coupons, each with a side length of 25 mm.

2.2. Electron microscopy and X-ray spectroscopy

Transmission Electron Microscopy (TEM) coupled with Energy Dispersive X-ray Spectroscopy (EDS) analyses were performed on

the bare Co sample. A Spin on Carbon (SoC) layer cured at 150 °C for 5 min was deposited as a protective layer. The aim was to study the morphology of Co thin film, atomic concentration of the elements and interfacial imperfections.

2.3. Reflectivity measurements

The reflectivity data was collected at the soft X-ray radiometry beamline (SX700) in the radiometry laboratory of the PTB, in the electron storage facility BESSY II [29–31]. The SX700 beamline is stationed at a bending magnet. The beamline was primarily designed to yield high and stable radiant power while the higher diffraction orders are suppressed. A selection of the beamline's parameters is indicated in Table 1.

A GaAsP photodiode was used as a detector. To reduce contamination effects, the beamline's reflectometer uses lubricant-free mechanics and is stationed in a clean-room environment.

The EUVR dataset studied here was measured in the angular range 8.0°–83.25° in the wavelength range 8.0–25.0 nm (corresponding to the energy range of ca. 155–49.5 eV). The wavelength-step in measuring the EUVR data was 0.1 nm between 8.0 nm and 18.0 nm, reduced to 0.04 nm between 18.04–20.0 nm and further reduced to 0.02 nm for the range above 20.0 nm to better sample the fine-structure expected in the optical constants. A total of 401 EUVR scans were taken. All the EUVR data we present here were measured in linear S-polarization.

X-ray Reflectivity (XRR) profiles were scanned at a wavelength of 1.595 nm (ca. 777.4 eV, Co L-absorption edge region) [33], to examine the structural stability of the capped sample. Another XRR profile was collected at 0.67 nm (ca. 1850 eV, Si K-absorption edge region) to aid in constructing the sample's model for the ADR inverse-problem.

Additionally, in the laboratories of optix fab GmbH (Jena), XRR profiles at Cu-Kα were collected in an X-ray diffractometer (D8 Discover by Bruker) from a twin of the bare Co sample to examine its structural stability.

3. Sample customization and characterization

Optimally, when targeting the determination of cobalt's optical constants using ADR, a bare elemental Co deposition would be coated on a Si-substrate. This has been attempted with a Co thin film with a nominal thickness of 30 nm. Unfortunately, the coating then suffered from strong oxidation and interdiffusion. Generally, thin films containing transition metals are known to develop (surface) oxidation layers. The problem with our Co sample was exacerbated because of the lasting oxidation growth and aging of the film. Over a period of around 30 weeks, sequentially collected XRR profiles of the bare Co deposition (on a Si substrate) were irreproducible.

To better address the aforementioned problem, High-Resolution Transmission Electron Microscopy (HRTEM) coupled with Energy-Dispersive Spectroscopy (EDS) analyses were carried out. The HRTEM images (Fig. 1) revealed heavy surface oxidation and a mixed layer consisting of buried oxidation and interdiffusion with the substrate. The buried oxidation developed due to the existence of oxygen in the substrate's native oxide.

For determining optical constants using ADR, this sample is undoubtedly difficult. One reason is the inverse-problem's sizeable dimensionality. In addition, Co has different oxidation states, such as CoO and Co_3O_4 and it is known to have its $M_{2,3}$ and $M_{4,5}$ transitions at ca. 21.4 nm (58 eV) [33,34]. With the corresponding absorption edge reported there [26], the accurate determination of optical constants from such a sample is futile. The expected chemical shifts with the resulting different and overlapping fine-structures due to the different oxidation states would make it perplexing for a robust determination of the optical constants. The situation is already exacerbated by the presence of the strong oxidation at the top to which the optical response is mostly sensitive. As well, the formation of cobalt-silicides (known from the EDS analysis) at the bottom adds to the problem.

The obstacles when determining optical constants from highly reactive materials using ADR and generally using other methods have been discussed before [35,36]. For example, to prevent the oxidation of reactive materials intended for TMM , Seely et al. (ref. [35]) demonstrated coating the film of the targeted reactive material with ultrathin protective layers, where the targeted film is to be coated over a photodiode directly. Kjornrattanawanich et al. (ref. [37]) further adapted that method where the targeted material is additionally coated over a protective tungsten underlayer over the photodiode. However, those techniques require multiple samples each of a different layer thickness regarding the targeted material [37]. Additionally, the accuracy of the calculated refractive index is still prone to inaccuracies due to the interpolations and extrapolations required to satisfy Kramers–Kronig formalism.

Another approach for ADR can be realized by coating the sample and conducting the measurements *in-situ* without breaking the vacuum [38]. This optimal approach is not widely accessible and, in our case, it would not practically allow verifying the

Table 1
Main parameters of the SX700 beamline at the standard settings [31,32].

Parameter	Approximate Value
Wavelength range	0.65–25 nm
Beam spot size (hor. • vert.)	1.0 • 1.0 mm^2
Beam divergence (hor. • vert.)	2.0 • 0.5 $mrad^2$
Linear polarization	98.7 %
Diffuse scattered light	0.2 %
Radiant power	0.5 μW at 13.5 nm
Relative bandwidth	Variable between 0.5×10^{-3} and 2.5×10^{-3}

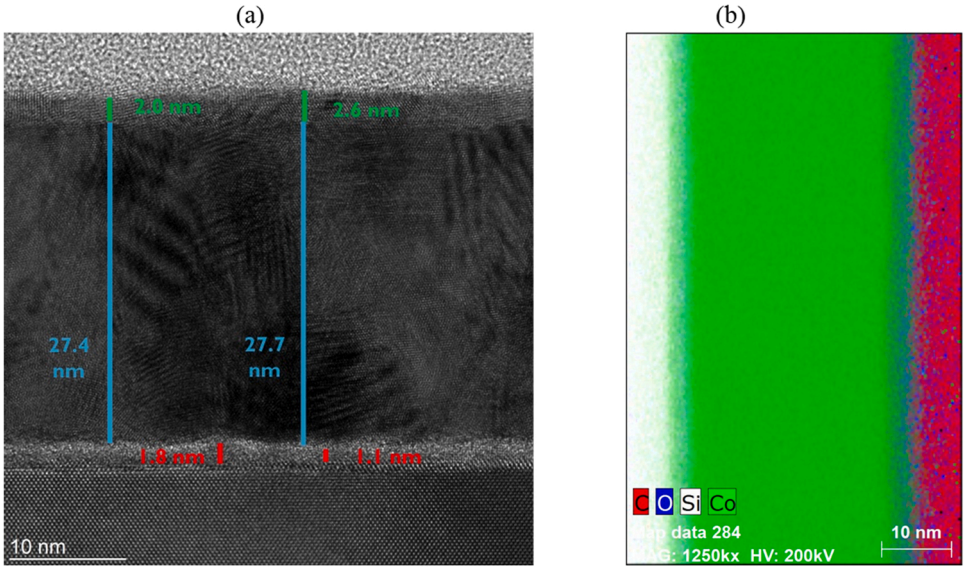

Fig. 1. Characterization of the bare Co film coated on a Si substrate. (a) HRTEM image. The green, blue and red lines mark selected local thicknesses of the oxide layer, the Co coating and the cobalt silicide (interdiffusion) layer, respectively. (b) Combined EDS chromatic map showing the distributions of C, O, Si and Co. The depth through the sample increases from right to left.

reproducibility of reflectivity profiles over extended periods. In principle, *in-situ* measurements will not help in preventing the interdiffusion between a Co deposition and a Si substrate.

Regarding a third approach, in some cases, determining the optical constants from oxidized samples is possible where the influence of oxidation can be considered. Delmotte et al. (ref. [39]) hinted a relevant issue with Cr thin films and reported the oxidation to become stable after months. In that case, determining the optical constants from oxidized Cr freestanding films using TMM was possible, where modelling the experimental data using oxidation layers with the stoichiometry Cr_2O_3 was feasible [39]. The case here with Co (see Fig. 1) is relatively more complicated. For our work, an alternative that suits ADR requirements – circumventing prolonged delays – is sought after to obtain a stable sample since it takes a relatively long time for a bare Co to become stable.

From our previous work on Co coatings [23], Ru has demonstrated the potential to serve as a diffusion barrier between Co and Si substrates. Ru is also known for its chemical stability and oxidation resistance [40], and its optical constants in the EUV have been extensively investigated before [41]. Thus, Ru is promising to be an underlayer for a Co coating but its relatively dense and highly absorbing for the EUV to also act as a capping layer here. On the other hand, Co and C are known to *pair well* as coatings for EUV MLMs applications [20]. When it comes to the optical constants, C is also one of the most investigated, for example see refs. [38,42–47]. Also, C-capping layers were used before for preventing oxidation of transition metals when determining the optical constants with ADR [48]. C as a top layer in Co/C MLMs proved to successfully prevent oxidation [49]. Based on that, another Co sample, a trilayer stratification where Co is sandwiched between C and Ru (Fig. 2), was fabricated.

Two measurements at Co-L edge energy were taken in a 6-week period to verify the structural stability of the capped sample. Fig. 3 shows the aging observed on a twin bare Co sample in comparison with the stable capped Co sample. The consistent reflectivity curves measured within six weeks are a clear indication of the stability of the capped sample. With the high elemental specificity of such reflectivity profiles, given its energy tuning with Co-L edge, this particularly emphasizes both structural and chemical stability of the capped sample. To the contrary, shown in Fig. 3(a), XRR profiles collected at Cu-Kα reveal vivid structural instability over time.

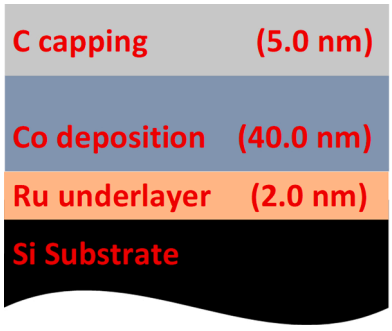

Fig. 2. A simplified sketch of the targeted nominal stratification of the customized multilayer Co sample.

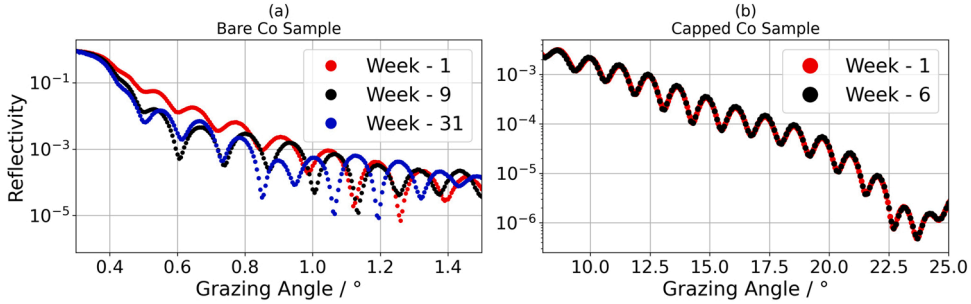

Fig. 3. Qualitative stability investigation of the two Co samples over time. (a) Three XRR measurements collected from a (twin) bare sample sequentially in a period of 30 weeks at a wavelength of 0.154 nm. (b) Two XRR measurements collected from the sample sequentially in a period of 6 weeks at a wavelength of 1.595 nm.

With the trilayer Co sample determined to be stable, another XRR profile at higher energy (0.67 nm) was collected and directly analysed using Time-Frequency Analysis (TFA) (Fig. 4). TFA are used to spare the trilayer Co sample from destructive characterization methods, such as TEM in the case of the bare sample. The Si K-edge energy is almost the highest available from our beamline, hence it will be the most suitable to describe the structural aspects of the sample, in comparison with the earlier presented measurements from the SX700 beamline.

TFA methods aim at resolving the characteristics of the stratification directly from the measured reflectivity profile's modulations (also known as Kiessig fringes [51]). For frequency analysis, the benefits of using the Fourier Transform (FT) for XRR analysis are well known [52], but FT has limitations. Considering a signal with frequencies components developing with time, FT assumes perfect periodicity of the signal and averages the frequencies distributions over the entire temporal domain. This leads to the fact that the time of occurrence of the individual frequencies cannot be determined. When using FT for investigating XRR profiles, this limitation translates to the inability to confirm the stratification order, where the layer thickness corresponds to the frequency in the aforementioned example. Another limitation is that FT spectra suffers from spectral noise and artefacts when transforming rapidly changing signals, and often XRR profiles are such. On the other hand, TFA methods offer a superior alternative enabling resolving not only the approximate thickness of the layers – given a multilayer sample – but also their stratification order. The applications of TFA methods on experimental XRR data are well known [50,53–62]. R. Clinciu proposed the idea in 1992 [55]. Smigiel et al. elaborated on the applicability of TFA for analyzing XRR data successfully in 1998 [53]. The Short-Time Fourier Transform (STFT), the Continuous Wavelet Transform (CWT) and the Wigner-Ville Distribution (WVD) are among the TFA methods used to study XRR profiles [↱50, ↱53-↱62]. The latter, the WVD is used here [63]. Examples and details on interpreting Time-Frequency Representations (TFRs), relevant for the TFA methods addressed earlier can be found in listed references [50,53,54].

Considering the WVD of the XRR profile (Fig. 4(b, c)), three features were resolved. With feature B resolved at the lowest diffraction

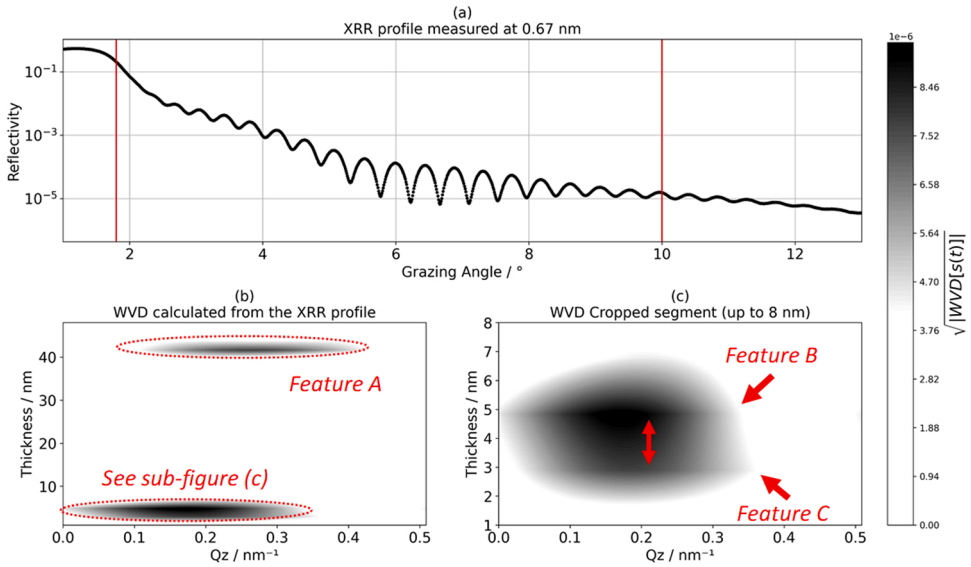

Fig. 4. Verification attempt of the trilayer stratification using the WVD. (a) XRR profile measured at Si K-edge. The vertical red lines mark the data segment taken for analysis. (b) Interpolated and filtered WVD contour plot calculated using mtspec Python wrappers (refs. [64,65]). (c) Cropped part from the contour plot shown in (b).

vector Q_z, it is assumed to indicate the uppermost layer. This interpretation is congruent with the intended fabrication settings, since a capping layer with a thickness of 5 nm is deposited on a 40 nm Co deposition. Moreover, features B and C are separable, given that the two layers are very thin, this is presumably due to the presence of Feature C below feature A.

Arguably, the attainment of the intended fabrication settings is supposed to be confirmed by the WVD TFR. The stability of the sample is verified with the sequential reflectivity measurements at Co L-edge energy. The outcomes of the TFR are only used here for initializing the relevant inverse-problem. Refining the structure model will follow with optimizing the EUVR data.

4. EUVR data analysis scheme

Although δ and β can be determined simultaneously for a given wavelength (range) from ADR data, the determination is carried out with an inverse-problem solving strategy. With determining optical constants from ADR data posing an ill-posed multi-minima optimization problem [66,67], classical optimization algorithms are prone to local minima entrapment yielding spurious best-fits. Also, even if the global minima were mapped, there are drawbacks in the results still. Only the best-fit values are indicated, the uncertainties and correlations of the target parameters are unavailable which is a shortcoming from a metrological point of view.

To better tackle the aforementioned difficulties, a robust scheme for determining the optical constants from ADR data is conducted with MCMC-based Bayesian inferences. MCMC-based Bayesian inferences are reviewed elsewhere [68], and have been used to study reflectivity data before [69–76].

Here, the inverse-problem is initialized with the probed sample's geometry modelled using discrete layers. In addition to the three layers depicted in Fig. 1, an ultrathin SiO_2 layer on top the substrate is modelled. This is known from fabrication, since the substrate's native oxide was not etched prior to sputtering Co.

The simulations required for the inverse-problem were calculated using Parratt's formalism combined with N évot-Croce factors to estimate the effects of interfacial imperfections [77,78]. The MCMC algorithm used here comes from the Python package emcee [79, 80]. More comprehensive details on the analysis scheme and on error modelling are given in refs. [↱62,81].

Ideally, the posterior distributions of both the structural parameters and the optical constants of each constituent of the tetralayer (on a substrate) system must be sampled, simultaneously. With our EUVR data consisting of 401 wavelength scans, the number of floating parameters would easily exceed 4000 given the tetralayer (on a substrate) model. An inverse-problem with this dimensionality would suffer numerous issues. R. Bellmann used the term "curse of dimensionality" to address relevant complications with optimizing high-dimensional inverse-problems [82,83]. To alleviate the curse of dimensionality, those optical constants of the substrate, the substrate's native oxide, and the Ru underlayer are to all be fixed. The optical constants of the substrate were taken from the CXRO database [12,84], and those of the native oxide and the Ru underlayer were taken from PTB's data [62,85]. Though the optical constants of C have been extensively investigated [12,14,38,42–46], disparities exist among the datasets (Fig. 5). The treatment then is to proceed with sampling the optical constants' posterior distributions of both C and Co alongside the structural parameters, except for the roughness of the substrate. The roughness of the super-polished substrate is known a priori to be below 1 Å Root-Mean-Square (RMS); hence it was fixed as 0.5 Å. However, the RMS value of the deepest interface is not expected to significantly alter the results.

The simulation attempt with sampling both posterior distributions of the optical constants of C and Co alongside the structural characteristics has been tried. Unfortunately, it yields spurious results in the spectral range above ca. 17 nm. Probably, this can be due to the shallow penetration depth of the used radiation, where the sensitivity of the EUVR profiles against some of the sampled parameters' posterior distributions are compromised. This is the case in particular for the structural characteristics of the Co coating since it additionally lays under a 5 nm capping layer. The penetration depth is further lessened due to the pronounced absorption of Co above ca. 17 nm, given the known M-absorption edge. When determining optical constants from thin films, the structural characteristics of the film are crucial to be accurately determined. In the EUV spectral range, materials are not only highly attenuating, but absorption increases significantly over small spectral steps. An automatic inferences procedure with equal weight *shares* considering

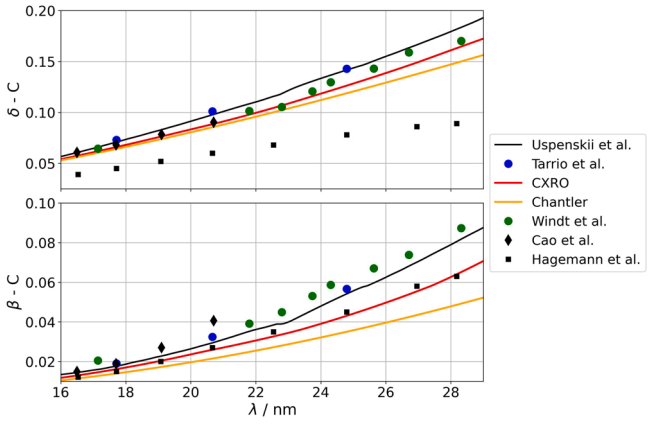

Fig. 5. Optical constants of C from seven datasets compared for the spectral range 14–29 nm [↱12, ↱14, ↱38, ↱42, 44–47]. The data labelled as Chantler was taken from ref. [47]. Top: δ values. Bottom: the extinction coefficients.

the sensitivity of the structural parameters for both *long* and *short* wavelengths can be misguided. For example, the sensitivity of an EUVR profile collected at wavelength of 8.0 nm to the structural characterises of the sample is much higher than that of a profile collected at wavelength of 25.0 nm. With that in mind, merely for the EUVR data collected up to 17.0 nm, the strategy now is to continue modelling the optical constants of both C and Co simultaneously, alongside the geometrical characteristics of the model. For the remaining data (the EUVR profiles collected between 17.1 nm and 25.0 nm) the parameters in the structural model will be fixed in the simulation as calculated from the data collected up to 17.0 nm. The aforementioned structural parameters are to be fixed except for the roughness parameter of the uppermost surface when conducting inferences from the segment collected between 18.0 nm and 25.0 nm, where it is considered a floating parameter because the latter segment was measured three weeks before the rest. This is important since the sample was exposed to the ambient air and the uppermost surface state must have been affected, where build-ups of contamination are expected. Also, the optical constants of Co will remain freely floating but those of C will be represented by an exponential function.

Upon sampling the posterior distributions of the parameters considering the EUVR data collected up to 17.0 nm, a plausible model describing the tetralayer stratification was obtained. The 91 wavelength scans (from 8.0 nm to 17.0 nm) were sampled globally to obtain the structural model. The obtained layers thicknesses (Fig. 6) are in good agreement with the nominal coating settings.

From the results shown in Fig. 6, the increase in the simulated capping layer is presumably due to contamination, since the sample was exposed to the ambient air after fabrication. The relatively high uncertainty of the thickness of the SiO_2 layer also has a physical interpretation. It is the deepest layer within the stratification. Due to the high absorption in the EUV spectral range and the related low penetration depth of radiation the sensitivity obviously decreases for the buried layers.

For the data collected above 17.0 nm, in all of the referenced optical constants literature values of C (Fig. 5) [12,14,38,42–46], the wavelength dependence of both β and δ is approximately an exponential function. This supports an assumption that C optical constants can be modelled as such. Modelling β and δ using functions significantly decreases the dimensionality of the inverse-problem and that is favourable in our case, especially when the experimental data does not exhibit reliable sensitivity for all parameters. That implies better stability and efficiency of the simulation in terms of computational effort. The addressed exponential function describing δ above 17.0 nm is defined as:

$$\delta^{approxi.}_{(17.1nm\rightarrow 25.0nm)}(\lambda) = \delta^{determined}_{(\lambda=17.0nm)}\zeta^{(17-\lambda)(0.125)} \tag{1}$$

Similarly, β is given as an exponential function. Resorting to such an approach (Eq. [(1)]) for modelling the optical constants of the carbonaceous capping layer spares sampling the probability distributions of 620 parameters. With 310 wavelength scans taken above 17.0 nm, ζ, a single freely floating parameter then addresses 310 parameters corresponding to δ values. Similarly, for η, as it relates to β values considering a similar exponential function. The values of δ and β determined at a wavelength of 17.0 nm are considered as fixed joining points for the simulation between the freely floating and the parameterized optical constants.

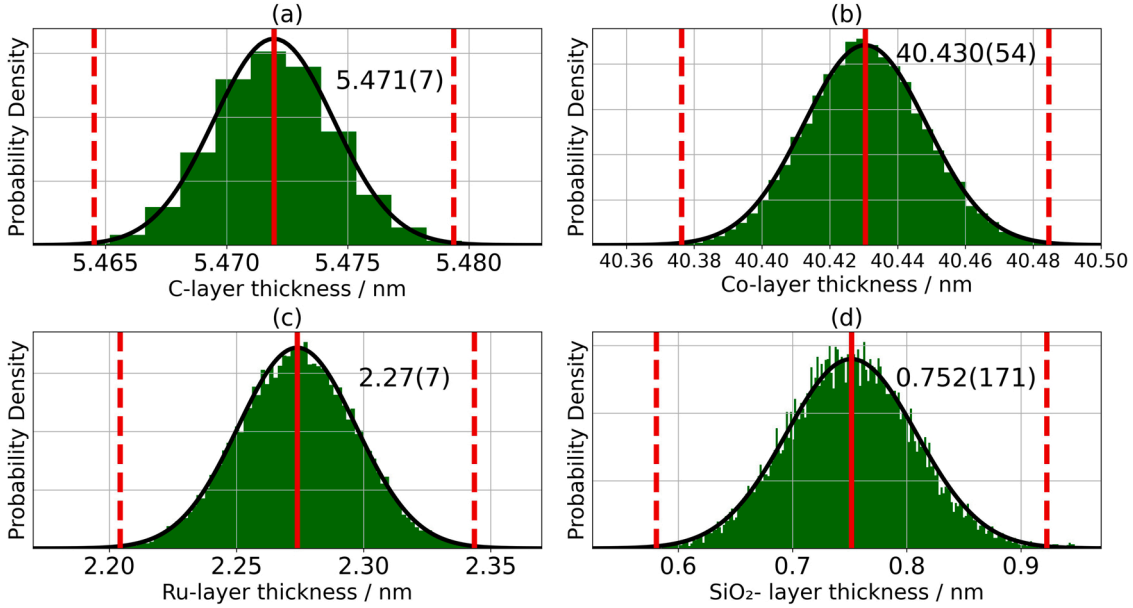

Fig. 6. The simulated layers thicknesses of the tetralayer stratification. The solid and dashed vertical lines mark the modes of the (fitted) Gaussian distributions, and a Confidence Interval (CI) of 3-σ, respectively. The layer thickness values are given with their corresponding uncertainties in the concise notation.

5. Determined optical constants and simulated EUVR

C has many allotropes, graphene, graphite, and diamond among others [86]. Pure C thin films also exist in an amorphous form. The electrical properties of some allotropes are distinctly different. For example, diamond is an insulator where graphene is a semi-conducting material. It is known that the electrical properties are directly linked to the optical constants. The fact that the properties of different C phases are disparate could be a reason for the differences in all of optical data shown in Fig. 5. It is possible that C films' crystalline order is highly susceptible to deposition settings, and easily varies. Hence, there seems to be no such a general *benchmark* dataset to verify the obtained optical constants of C. Nevertheless, the obtained optical constants from both segments of the EUVR data (up to 17.0 nm and above) depict a convincing trend (Fig. 7).

Fundamentally, we do not present the optical constants determined for the carbonaceous capping layer as such for elemental C. The characteristics of the capping layer were not investigated considering the stoichiometry and crystallinity. As mentioned before, this is significant for C given its allotropism [86]. The phase(s) present in the capping layer and the crystalline order are not known certainly. Additionally, the simulation model does not include a separate contamination layer that would estimate the effects of the inevitable contamination and oxidation, which are known to occur. This effectively affects the calculated optical constants of the carbonaceous capping layer.

A key advantage obtained using MCMC-based Bayesian inferences is the ability to probe cross-correlations. Estimating such inter-dependencies of the sampled posterior distributions greatly helps in evaluating the analysis scheme. The covariances and correlations to selected parameters are shown in Fig. 8.

To satisfy the used MCMC-based Bayesian inferences framework, a prior range addressing the possible solution space to be sampled has to be defined. This range had been defined around the tabulated values of the CXRO [12]. However, for the optical constants of Co above 19.0 nm, priors with box shapes constraining the intervals [−0.35,0.15] and [0.05,0.35] for δ and β, respectively, were defined. Although the prior range is enormous, the framework proved to yield plausible results (Fig. 9 and Fig. 10). Also, the simulated EUVR data resembles the measurements quite well (Fig. 11).

The results of this work (Fig. 9), regarding β, are in some agreement with other literature values [↱12-↱14]. The correspondence in the shown data is noticeable with β peaking at ca. 20 nm, and generally with tracing the fine-structure around the M-absorption edge, except for Chantler's tabulations [14]. However, there are significant differences considering δ (Fig. 10). Valencia et al. data (ref. [89]) demonstrates a good agreement with our results concerning the fine-structure behaviour of the extinction coefficients between ca. 16.5 nm and 18.5 nm. Nevertheless, pronounced divergence occurs above ca. 22 nm. Willems et al. data (Ref. [28]) is the most recent among the addressed literature values, it demonstrates a very good agreement if scaled up with a factor of ca. 1.08. Probably, this could be due to density difference. Valencia et al. and Willems et al. also reported using capping layers to prevent oxidation [28,89]. The presence of a variable fine-structure in our results and in the two latter reports could indicate that oxidation might obscure resolving such features.

The relatively larger differences in δ's values could be due to the inaccuracies corelated with the estimations made to enable Kramer-Kronig analysis. Generally, for different elements, significant inconsistencies between different optical constants datasets have been reported before [90–93]. There can be numerous reasons for inconsistencies to occur. One example that could give a clue here is the case of copper [90]. Brimhall et al. (Ref. [90]) demonstrated the reason behind the inconsistencies with the results found in Haensel

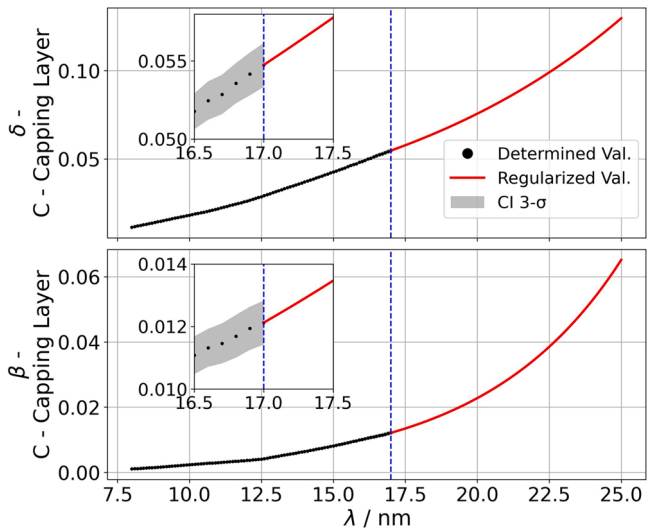

Fig. 7. The calculated optical constants of the capping layer. Top: δ values. Bottom: the extinction coefficients. The sub-plots emphasize the continuity in the calculated values where exponential functions were used to model the responses above 17.0 nm. Up to 17.0 nm, the optical constants' posterior distributions were sampled in their prior ranges without any constraints and the CIs are shown. The blue lines mark the boundary between the individually determined values and those parameterized with exponential functions.

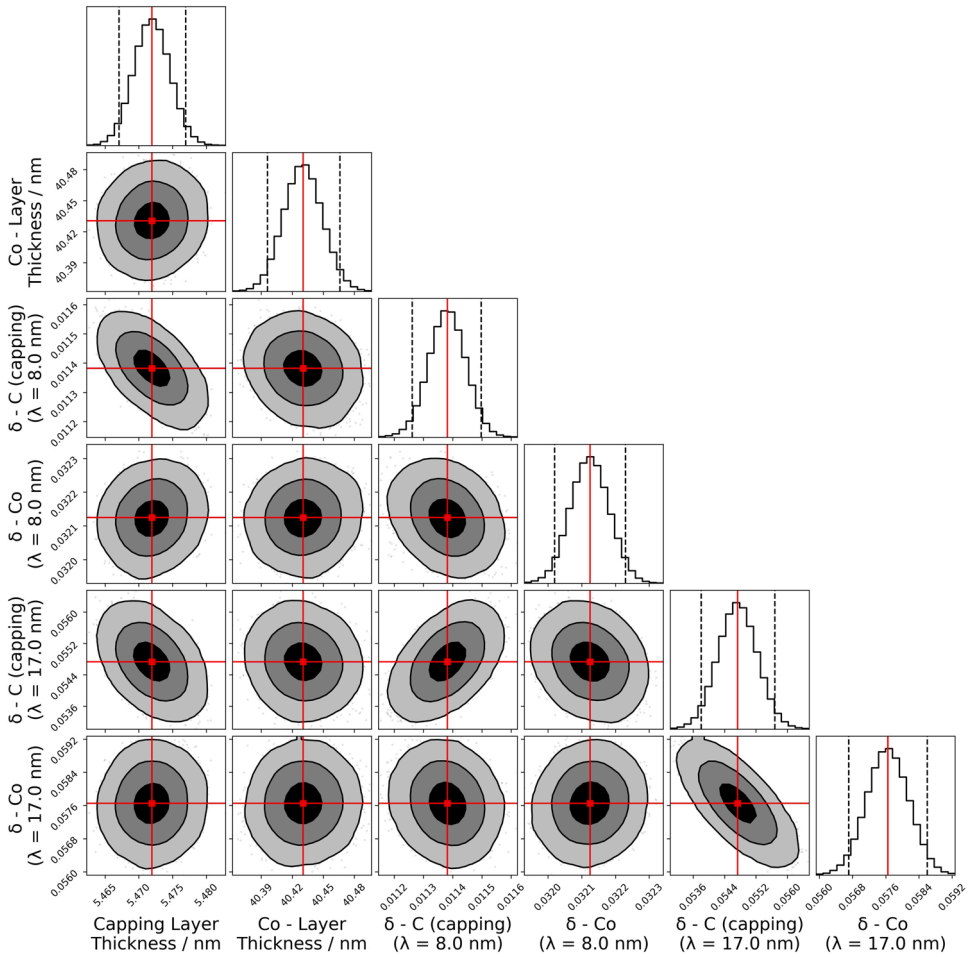

Fig. 8. Corner plot of the posterior distributions from six selected parameters. For the 1-D histograms, the (fitted Gaussian) distributions' modes are marked by red lines. Vertical dashed black lines mark the CI of 3-σ. The three levels observed in the 2-D histograms reveals the 1, 2, and 3- σ density regions [87,88].

et al. (Ref. [94]) and Hagemann et al. (Ref. [46]) to be the accidental oxidation of the sample investigated in the two latter works [90]. Co is also prone to oxidation. As demonstrated with the bare Co sample presented in this work, strong interdiffusion with the Si substrate adds to the issue. Bruhn et al. (Ref. [95]) showed that absorption spectra of the atomic and metallic states of cobalt among other transition metals are different. Ultrathin films made of Co might not exhibit the fully metallic response, given the scaling effects. Nevertheless, a *presumptionless* explanation would require the systematic characterization of the samples investigated in the addressed works.

The discrepancies between our results and Chantler's predictions (ref. [14]) are interesting. Addressing such a comparison can lead improving the theoretical formalisms used in predicting the optical responses of transition metals, concerning the EUV spectral range.

Coming to the simulated EUVR data, a fine fitting is demonstrated (Fig. 11 and 12). The abrupt changes observed in the residual map (Fig. 11 (c)) starting at 18.0 nm are (presumably) due to the fact that the data above 18.0 nm were measured 17 days before the data between 8.0.0 nm and 17.9 nm, during which the sample was not in vacuum. Hence, slight differences in the surface state due to contamination can be critical in the optical response at this spectral range. These indicated differences are the main reason for using lubricant-free mechanics in the beamline's reflectometer. Yet, no measures can completely avoid hydrocarbon contamination known to affect EUV measurements.

At this point, it is crucial to distinguish between the stability of the stratification and environmental contamination. The former has been demonstrated with XRR measurements. Reflectivity profiles collected with a photon energy at Co-L edge matched for a 6-week period of time. Such profiles are extremely sensitive to Co but not to an ultrathin atomic layer of hydrocarbons.

A different perspective to emphasize the agreement between the measurements and the simulations is shown in Fig. 12.

Ideally, the effects of physiosorbed and chemisorbed molecules on the surface have to be included in the model. Unfortunately, given the addressed high dimensionality of the problem, abstractly adding additional free parameters is a dubious solution. The presented simulated tetralayer (on a substrate) model is understood to be a simplified, but a plausible one. Using discrete layer-modelling, each layer was represented with an ideal density profile. The used formalism (of Parratt's, ref. [77]) to calculate

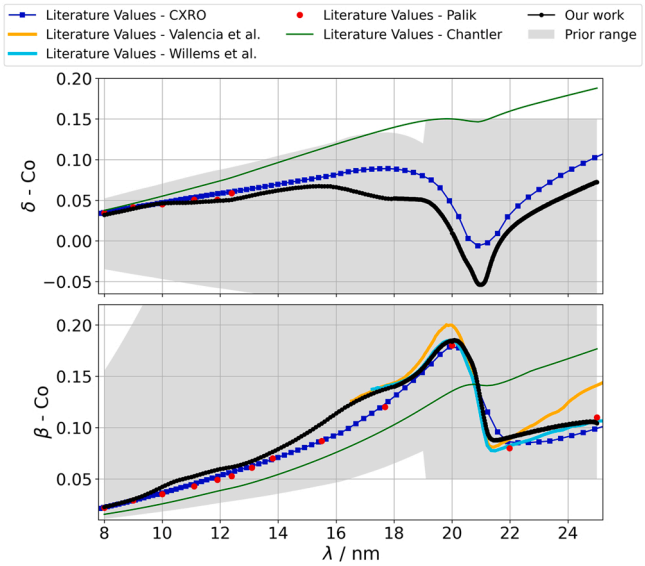

Fig. 9. The calculated optical constants of Co, with comparison to literature data [12–14,28,47,89]. Top: δ values. Bottom: the extinction coefficients. The appearing black line actually consists of 401 closely spaced data points.

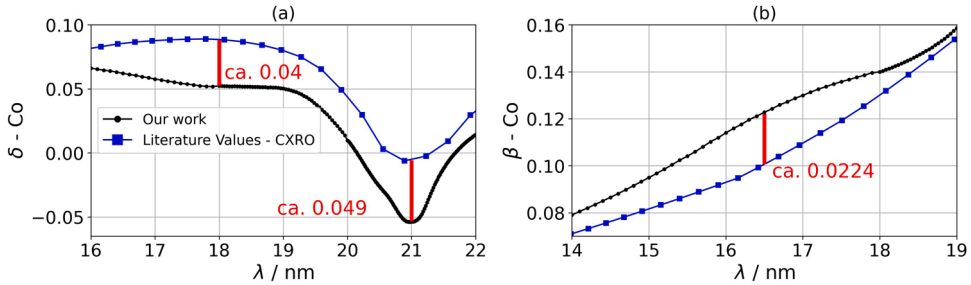

Fig. 10. Comparison between the calculated optical constants of Co in our work with CXRO's tabulations [12]. (a) δ values. The red lines mark the absolute difference at the wavelengths of 18.0 nm and 21.0 nm. (b) The extinction coefficients. The red line marks the absolute difference at the wavelength of 16.5 nm.

reflectivity additionally assumes ideal lateral uniformity of the films' bodies. However, the existent structure probably has defects and would possess non-ideal vertical and lateral density profiles. Addressing such intricate structural aspects can lead to creating a problem with an aggravated curse of dimensionality. A relatively similar discussion on the optimization of reflectivity data is given in ref. [96]. Even excluding such intricate details, as mentioned before, the number of free parameters would exceed 4000 if no parameterization or substitution measures were taken. Arguably, about ADR as a method for determining optical constants, the required inverse-problem is the main drawback. Therefore, approximations were taken, such as modelling the optical constants of C above 17.0 nm with an exponential function and assuming the density profiles of the layers to be uniform.

6. Conclusions and perspectives

A significant outcome of our work is demonstrating the ability of the used computational scheme to deliver reliable results for inverse-problems with overwhelming prior ranges. Generally, for Bayesian inferences, when the prior knowledge about a parameter in an inverse-problem is vague, the assumed convergence of the problem is challenged where the sampling efficiency can be relatively insufficient. When an algorithm targets the convergence for an optimization parameter, as the *search space* of its posterior distribution gets larger, multi-modalities are likely to occur and the time needed for the inferences algorithm to probe the entire parameter space can be beyond convenience. Regarding the M-absorption edge region, there are no accurate data for the refractive indices (δ) values of Co. The shaded prior ranges shown in Fig. 9 illustrate. Still, the used framework yielded noiseless results for calculated values varying over orders of magnitude, although requiring an extensive computational power. It is particularly useful to demonstrate resolving a fine structure with MCMC-based Bayesian inferences, since determining optical constants in the vicinity of absorption edges is known to be quite challenging. For example, the determined optical constants over energy ranges containing absorption edges are particularly vulnerable to the spectral resolution of the used setup [97].

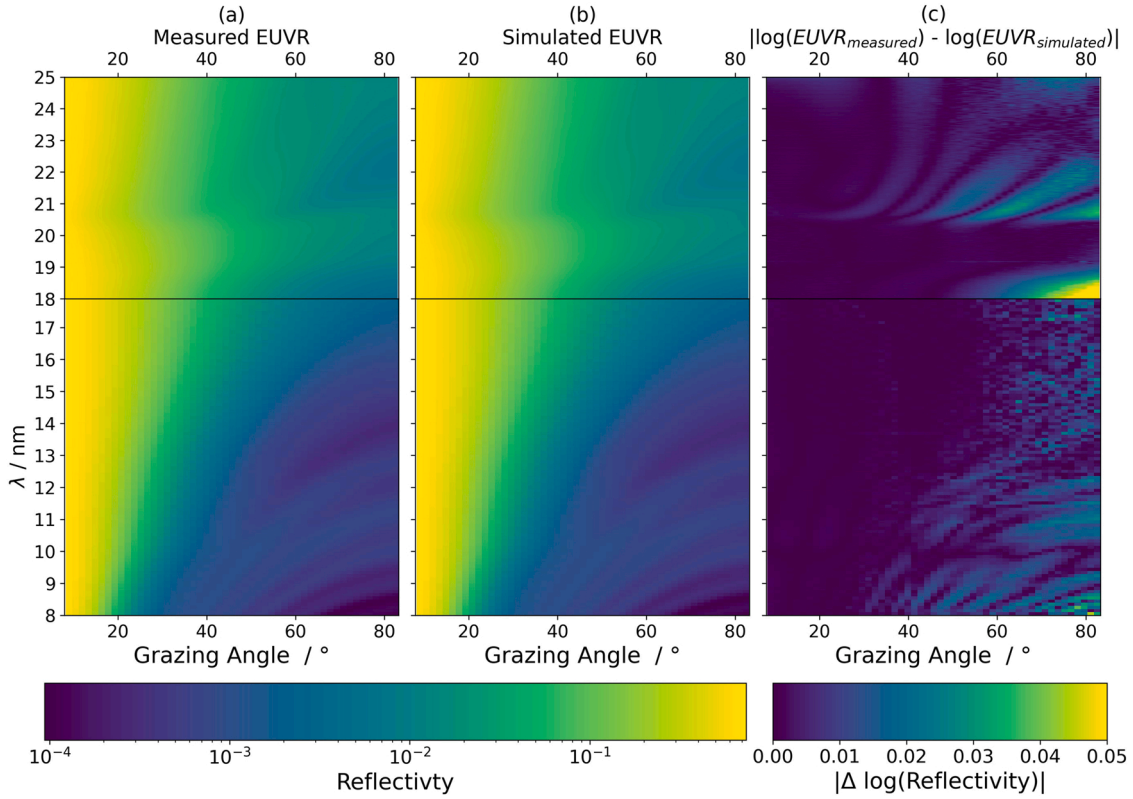

Fig. 11. (a) measured data (b) simulated EUVR map (c) mapping of the residual between the measured and the simulated EUVR.

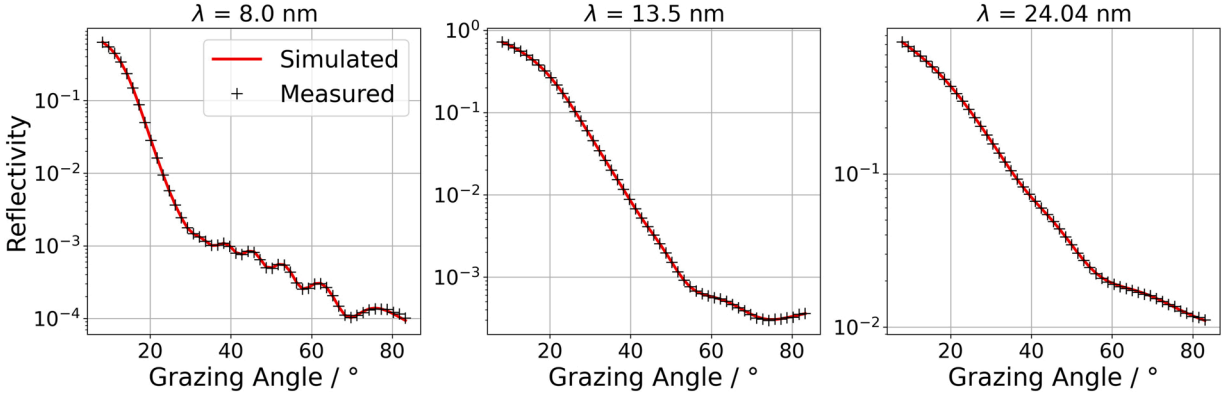

Fig. 12. The measured and the simulated reflectivity from the multilayer Co sample at three selected wavelengths.

A note on the uncertainties calculated from the MCMC-based Bayesian inferences; they are not absolute given the measurements. The uncertainties addressed here are merely congruent with the used model. That is emphasised since a different model for the inverse-problem would lead to different results.

The insight in the investigations here of Co thin films is generally very useful. For example, cobalt's oxidation kinetics [98], cobalt-silicide growth [99], among other phenomena were studied before. Here, additionally, counter measures against oxidation and silicides growth are tested.

Our results can also be useful for further investigating the MCD at the M-absorption edge of Co [100], among other magneto-optical effects. Co magneto-optical response in the vicinity of the M-absorption as a ferromagnetic material edge attracted attention [28,89,101]. To serve that purpose, the extinction coefficients were experimentally determined at the M-absorption edge [28], but the refractive indices were not given. Yet, accurate refractive indices are needed to better understand the magneto-optical response.

The used software here is Open Source [64,65,79,80,87,88,102,103]. The determined optical constants in this work are available

on the PTB's online Optical Constants Database (OCDB); < www.ocdb.ptb.de/home >.

Declaration of Competing Interest

The authors declare that they have no known competing financial interests or personal relationships that could have appeared to influence the work reported in this paper.

Data Availability

Data will be made available on request.

Acknowledgements

This project has received funding from the Electronic Component Systems for European Leadership Joint Undertaking under grant agreement No 783247 – Technology Advances for Pilot line of Enhanced Semiconductors for 3 nm (TAPES3) and from the European Metrology Programme for Innovation and Research (EMPIR) programme under grant No 20IND04 - Traceable Metrology of Soft X-ray to IR Optical Constants and Nanofilms for Advanced Manufacturing (ATMOC). These Joint Undertakings receive support from the European Union's Horizon 2020 research and innovation program and from Netherlands, France, Belgium, Germany, Czech Republic, Austria, Hungary, Israel, Switzerland, Turkey, Denmark and Finland. Also, the authors would like to thank Olivier Richard from Materials and Component Analysis (MCA) department at imec for TEM and EDS reports.

References

[1] C. Zahlten, P. Gräupner, J. van Schoot, P. Kürz, J. Stoeldraijer, W. Kaiser, High-NA EUV lithography: pushing the limits, Proc. SPIE 11177 35th Eur. Mask. Lithogr. Conf. 111770B (2019).
[2] J. Van Schoot, S. Lok, E. van Setten, R. Maas, K. Troost, R. Peeters, J. Finders, J. Stoeldraijer, J. Benschop, P. Graeupner, P. Kuerz, W. Kaiser, High-NA EUV lithography exposure tool: advantages and program progress, Proc. SPIE 11517 Extrem. Ultrav. Lithogr. 2020 (2021), 1151712.
[3] T. Luu, M. Garg, S. Kruchinin, A. Moulet, M. Hassan, E. Goulielmakis, Extreme ultraviolet high-harmonic spectroscopy of solids, Nature 521 (2015) 498–502.
[4] S. Bogachev, N. Chkhalo, S. Kuzin, D. Pariev, V. Polkovnikov, N. Salashchenko, S. Shestov, S. Zuev, Advanced materials for multilayer mirrors for extreme ultraviolet solar astronomy, Appl. Opt. 55 (9) (2016) 2126–2135.
[5] L. Bahrenberg, S. Danylyuk, S. Glabisch, M. Ghafoori, S. Schröder, S. Brose, J. Stollenwerk, P. Loosen, Characterization of nanoscale gratings by spectroscopic reflectometry in the extreme ultraviolet with a stand-alone setup, Opt. Express 28 (14) (2020) 20489–20502.
[6] M. Tanksalvala, C. Porter, Y. Esashi, B. Wang, N. Jenkins, Z. Zhang, G. Miley, J. Knobloch, B. McBennett, N. Horiguchi, S. Yazdi, J. Zhou, M. Jacobs, C. Bevis, R. Karl Jr., P. Johnsen, D. Ren, L. Waller, D. Adams, S. Cousin, C.-T. Liao, J. Miao, M. Gerrity, H. Kapteyn, M. Murnane, Nondestructive, high-resolution, chemically specific 3D nanostructure characterization using phase-sensitive EUV imaging reflectometry, Sci. Adv. 7 (5) (2021) 1–11.
[7] P. Wachulak, A. Bartnik, M. Duda, T. Fok, Ł. Węgrzyński, D. Adjei, M. Ayele, L. Vysin, and H. Fiedorowicz, Generation and selected applications of the EUV and SXR radiation, emitted from compact laser-plasma sources, OSA High-brightness Sources and Light-driven Interactions Congress 2020 (2020) paper ETu1A.1.
[8] M. Tryus, Extreme Ultraviolet Reflectometry for Structural and Optical Characterization of Thin Films and Layer Systems, PhD thesis, Fakultät für Mathematik, Informatik und Naturwissenschaften der RWTH Aachen University, 2018.
[9] R. Soufli, Optical constants of materials in the EUV/soft x-ray region for multilayer mirror applications, PhD thesis, University of California, Berkeley, 1997.
[10] W. Hunter, Measuring optical constants from the UV to x-ray wavelengths: how it was (and is) done, Proc. SPIE 5538 Opt. Constants Mater. UV X-Ray Wavel. (2004) 1–16.
[11] E. Spiller, Soft X-ray optics, SPIE, 1994, pp. 5–21.
[12] B. Henke, E. Gullikson, and J. Davis, X-Ray interactions: photoabsorption, scattering, transmission, and reflection at E = 50–30,000 eV, Z = 1–92, At. Data Nucl. Data Tables 54(2), (1993) 181–342. Updates to the tabulated value are accessible in the CXRO online database via; < https://henke.lbl.gov/optical_constants/asf.html >.
[13] E. Palik, Handbook of Optical Constants of Solids, vol. 2, Academic press, 1998.
[14] C. Chantler, Theoretical form factor, attenuation, and scattering tabulation for Z=1–92 from E=1–10 eV to E=0.4–1.0 MeV, J. Phys. Chem. Ref. Data 24 (1) (1995) 71–642.
[15] A. Kaloyeros, Y. Pan, J. Goff, B. Arkles, Review—Cobalt thin films: trends in processing technologies and emerging applications, ECS J. Sol. Sta. Sci. Tech. 8 (2) (2019) P119–P152.
[16] E. Spiller, D. Stearns, M. Krumrey, Multilayer x-ray mirrors: Interfacial roughness, scattering, and image quality, J. Appl. Phy 74 (1) (1993) 107–118.
[17] K. Le Guen, M.-H. Hu, J.-M. André, P. Jonnard, S.K. Zhou, H. Ch. Li, J. Zhu, Z. Wang, C. Meny, Development and interfacial characterization of Co/Mg periodic multilayers for the EUV range, J. Phys. Chem. C 114 (14) (2010) 6484–6490.
[18] P. Jonnard, Z.-S. Wang, J.-T. Zhu, C. Meny, J.-M. André, M.-H. Hu, K. Le Guen, Characterization of multilayers and their interlayers: application to Co-based systems, Chin. Opt. Lett. COL 11 (Suppl) (2013), S10601.
[19] P. Yuan, Characterization of physico-chemical environment of Co-based multilayer mirrors working in the soft x-ray and EUV ranges, PhD thesis, Université Pierre et Marie Curie, 2014.
[20] N. Kolachevsky, E. Louis, E. Spiller, M. Mitropol'skii, F. Bijkerk, E. Ragozin, Spectral characteristics of multilayer cobalt—carbon mirrors for the λ≈ 7.5 nm range, Quant. Elec. 27 (8) (1997) 712–716.
[21] E. Spiller, K.-B. Youn, Studies toward the optimization of ion polishing for multilayer x-ray mirrors, Multilayer and Grazing Incidence X-Ray/EUV Optics II, Proc. SPIE 2011 (1994) 288–298.
[22] J. Feng, Q. Huang, R. Qi, A. Sokolov, M. Sertsu, X. Yang, Z. Zhang, Z. Wang, High reflectivity Co/Mg multilayer working in the broad soft x-ray range of 350–770 eV, J. Phy. D: Appl. Phys. 55 (17) (2022), 175107.
[23] V. Philipsen, K. Luong, L. Souriau, E. Hendrickx, A. Erdmann, D. Xu, P. Evanschitzky, R. van de Kruijs, A. Edrisi, F. Scholze, C. Laubis, M. Irmscher, S. Naasz, C. Reuter, Reducing EUV mask 3D effects by alternative metal absorbers, Proc. SPIE 10143, Extrem. Ultrav. (EUV) Lithogr. VIII (2017), 1014310.
[24] F. Scholze, C. Laubis, K. Vu Luong, V. Philipsen, Update on optical material properties for alternative EUV mask absorber materials, Proc. SPIE 10446, 33rd Eur. Mask. Lithogr. Conf. (2017), 1044609.
[25] D. Thakare, M. Wu, K. Opsomer, C. Detavernier, P. Naujok, Q. Saadeh, V. Soltwisch, A. Delabie, V. Philipsen, Evaluation of Ta-Co alloys as novel high-k EUV mask absorber, Proc. SPIE 12051 Opt. EUV Nanolithogr. XXXV 120510D (2022).

[26] B. Sonntag, R. Haensel, C. Kunz, Optical absorption measurements of the transition metals Ti, V, Cr, Mn, Fe, Co, Ni in the region of 3p electron transitions, Sol. St. Comm. 7 (8) (1969) 597–599.
[27] P. Grychtol, R. Adam, S. Valencia, S. Cramm, D. Bürgler, C. Schneider, Resonant magnetic reflectivity in the extreme ultraviolet spectral range: Interlayer-coupled Co/Si/Ni/Fe multilayer system, Phys. Rev. B 82 (2010), 054433.
[28] F. Willems, S. Sharma, C. v Korff Schmising, J. Dewhurst, L. Salemi, D. Schick, P. Hessing, C. Strüber, W. Engel, S. Eisebitt, Magneto-optical functions at the 3 p resonances of Fe, Co, and Ni: Ab initio description and experiment, Phys. Rev. Lett. 122 (21) (2019), 217202.
[29] F. Scholze, B. Beckhoff, G. Brandt, R. Fliegauf, A. Gottwald, R. Klein, B. Meyer, U. Schwarz, R. Thornagel, J. Tuemmler, K. Vogel, J. Weser, G. Ulm, High-accuracy EUV metrology of PTB using synchrotron radiation, Proc. SPIE 4344 (2001) 402–413.
[30] C. Laubis, A. Kampe, C. Buchholz, A. Fischer, J. Puls, C. Stadelhoff, F. Scholze, Characterization of the polarization properties of PTB's EUV reflectometry system, Proc. SPIE 7636 (2010) 76362R.
[31] M. Richter, G. Ulm, Metrology with synchrotron radiation–a brief introduction, PTB-Mitt. 124 (3) (2004) 3–6.
[32] A. Haase, Multimethod Metrology of Multilayer Mirrors Using EUV and X-Ray Radiation, PhD thesis, Technische Universität Berlin, Inst. Optik und Atomare Physik (2017) 38–41.
[33] G. Zschornack, Handbook of X-ray data, Springer Science & Business Media, 2007, p. 229.
[34] Y. Lykhach, S. Piccinin, T. Skála, M. Bertram, N. Tsud, O. Brummel, M. Camellone, K. Beranová, A. Neitzel, S. Fabris, K. Prince, V. Matolín, J. Libuda, Quantitative analysis of the oxidation state of cobalt oxides by resonant photoemission spectroscopy, J. Phys. Chem. Lett. 10 (20) (2019) 6129–6136.
[35] J. Seely, Y. Uspenskii, B. Kjornrattanawanich, D. Windt, Coated photodiode technique for the determination of the optical constants of reactive elements: La and Tb, Proc. SPIE 6317, Adv. X-Ray/ EUV Opt., Compon. Appl. 63170T (2006).
[36] Y. Uspenskii, J. Seely, N. Popov, A. Vinogradov, Yu Pershin, V. Kondratenko, Efficient method for the determination of extreme-ultraviolet optical constants in reactive materials: application to scandium and titanium, J. Opt. Soc. Am. A 21 (2) (2004) 298–305.
[37] B. Kjornrattanawanich, D. Windt, J. Seely, Optical constants determination of samarium, holmium, and erbium in the 1.5–850 eV spectral range using a transmittance method, Appl. Opt. 49 (31) (2010) 6006–6013.
[38] C. Tarrio, R. Watts, T. Lucatorto, J. Slaughter, C. Falco, Optical constants of in situ-deposited films of important extreme-ultraviolet multilayer mirror materials, Appl. Opt. 37 (19) (1998) 4100–4104.
[39] F. Delmotte, J. Meyer-Ilse, F. Salmassi, R. Soufli, C. Burcklen, J. Rebellato, A. Jérome, I. Vickridge, E. Briand, E. Gullikson, Soft x-ray optical constants of sputtered chromium thin films with improved accuracy in the L and M absorption edge regions, J. Appl. Phys. 124 (2018), 035107.
[40] S. Bajt, Z. Dai, E. Nelson, M. Wall, J. Alameda, N. Nguyen, S. Baker, J. Robinson, J. Taylor, A. Aquila, N. Edwards, Oxidation resistance and microstructure of ruthenium-capped extreme ultraviolet lithography multilayers, J. Micro/Nanolithogr. MEMS MOEMS 5 (2) (2006), 023004.
[41] U. Schlegel, Determination of the optical constants of Ruthenium in the EUV and soft x-ray region using synchrotron radiation, Diploma thesis, Technische Fachhochschule Berlin, 2000.
[42] Y. Uspenskii, J. Seely, B. Kjornrattanawanich, D. Windt, Ye Bugayev, V. Kondratenko, I. Artyukov, A. Titov, E. Kulatov, A. Vinogradov, Determination of the optical constants of amorphous carbon in the EUV spectral region 40–450 eV, Proc. SPIE 6317 Adv. X-Ray/EUV Opt. Compon. Appl. (2006), 631713.
[43] I. Diel, J. Friedrich, C. Kunz, S. Di Fonzo, B. Müller, W. Jark, Optical constants of float glass, nickel, and carbon from soft-x-ray reflectivity measurements, Appl. Opt. 36 (25) (1997) 6376–6382.
[44] D. Windt, W. Cash, M. Scott, P. Arendt, B. Newnam, R. Fisher, A. Swartzlander, P. Takacs, J. Pinneo, Optical constants for thin films of C, diamond, Al, Si, and CVD SiC from 24 Å to 1216 Å, Appl. Opt. 27 (2) (1988) 279–295.
[45] J. Cao, M. Yanagihara, M. Yamamoto, Y. Goto, T. Namioka, Simultaneous determination of the optical constants and thickness of very thin films by using soft-x-ray reflectance measurements, Appl. Opt. 33 (10) (1994) 2013–2017.
[46] H.-J. Hagemann, W. Gudat, C. Kunz, Optical constants from the far infrared to the x-ray region: Mg, Al, Cu, Ag, Au, Bi, C, and Al2O3, J. Opt. Soc. Am. 65 (6) (1975) 742–744.
[47] The XrayDB Python package. Accessible via; < https://xraypy.github.io/XrayDB/ >.
[48] N. Kiharaand, H. Nagata, N. Nakagiri, H. Fujisaki, T. Miyahara, Optical constants for coated thin films in the soft x-ray region, Rev. Sci. Inst. 60 (1989) 2227–2230.
[49] E. Jiang, H. Bai, R. Tian, C. Wang, Aging effect of Co/C soft x-ray multilayer mirrors, J. Appl. Phys. 81 (1) (1997) 184–189.
[50] K. Sakurai, M. Mizusawa, M. Ishii, Significance of frequency analysis in X-ray reflectivity: towards analysis which does not depend too much on models, Trans. Mater. Res. Soc. Jpn. 33 (3) (2008) 523–528.
[51] H. Kiessig, Interferenz von Röntgenstrahlen an dünnen Schichten, Ann. Phys. 402 (7) (1931) 769–788.
[52] J. Wernecke, A. Shard, M. Krumrey, Traceable thickness determination of organic nanolayers by X-ray reflectometry, Surf. Interface Anal. 46 (10–11) (2014) 911–914.
[53] E. Smigiel, A. Knoll, N. Broll, A. Cornet, Determination of layer ordering using sliding-window Fourier transform of x-ray reflectivity data, Model. Simul. Mater. Sci. Eng. 6 (1) (1998) 29–34.
[54] E. Smigiel, A. Cornet, Characterization of a layer stack by wavelet analysis on x-ray reflectivity data, J. Phys. D: Appl. Phys. 33 (15) (2000) 1757–1763.
[55] R. Clinciu, The application of the Wigner distribution function to X-ray reflectivity, M.S. thesis. Department of Engineering, University of Warwick,, 1992.
[56] B. Tanner, D. Bowen, X-Ray Metrology in Semiconductor Manufacturing, CRC, 2006, p. 253.
[57] I. Prudnikov, R. Matyi, R. Deslattes, Wavelet transform approach to the analysis of specular x-ray reflectivity curves, J. Appl. Phys. 90 (7) (2001) 3338–3346.
[58] O. Durand, N. Morizet, Fourier-inversion and wavelet-transform methods applied to X-ray reflectometry and HRXRD profiles from complex thin-layered heterostructures, Appl. Surf. Sci. 253 (1) (2006) 133–137.
[59] H. Jiang, A. Michette, S. Pfauntsch, Z. Wang, D. Li, Applications of wavelet analysis to study growth characteristics of x-ray multilayer mirrors, J. Phys. D: Appl. Phys. 44 (2011), 435303.
[60] O. Starykov, K. Sakurai, Determination of interface roughness of Gd films deposited on Si surface using improved wavelet transform of X-ray reflectivity data, Appl. Surf. Sci. 244 (2005) 235–239.
[61] R. Deslattes, R. Matyi, Analysis of thin-layer structures by X-Ray reflectometry. Handbook of Silicon Semiconductor Metrology, 1st edition, CRC Press, 2001, pp. 807–809.
[62] Q. Saadeh, P. Naujok, V. Philipsen, P. Hönicke, C. Laubis, C. Buchholz, A. Andrle, C. Stadelhoff, H. Mentzel, A. Schönstedt, V. Soltwisch, F. Scholze, Time-frequency analysis assisted determination of ruthenium optical constants in the sub-EUV spectral range 8nm – 23.75nm, Opt. Express 29 (25) (2021) 40993–41013.
[63] G. Matz, F. Hlawatsch, Wigner distributions (nearly) everywhere: time–frequency analysis of signals, systems, random processes, signal spaces, and frames, Sig. Proc. 83 (7) (2003) 1355–1378.
[64] G. Prieto, R. Parker, F. Vernon, A Fortran 90 library for multi taper spectrum analysis, Com. Geo. 35 (8) (2009) 1701–1710.
[65] L. Krischer, mtspec Python wrappers 0.3.2, Zenodo (2016), https://doi.org/10.5281/zenodo.321789.
[66] M. Hobson, J. Baldwin, Markov-chain Monte Carlo approach to the design of multilayer thin-film optical coatings, Appl. Opt. 43 (13) (2004) 2651–2660.
[67] W. Wild, H. Buhay, Thin-film multilayer design optimization using a Monte Carlo approach, Opt. Lett. 11 (11) (1986) 745–747.
[68] R. van de Schoot, S. Depaoli, R. King, B. Kramer, K. Märtens, M. Tadesse, M. Vannucci, A. Gelman, D. Veen, J. Willemsen, C. Yau, Bayesian statistics and modelling, Nat. Rev. Meth. Prim. 1 (1) (2021) 1–26.
[69] D. Windover, D. Gil, J. Cline, A. Henins, N. Armstrong, P. Hung, S. Song, R. Jammy, A. Diebold, NIST method for determining model-independent structural information by X-ray reflectometry, AIP Conf. Proc. 931 (1) (2007) 287–291.
[70] B. Treece, P. Kienzle, D. Hoogerheide, C. Majkrzak, M. Lösche, F. Heinrich, Optimization of reflectometry experiments using information theory, J. Appl. Cryst. 52 (2019) 47–59.
[71] A. Nelson, S. Prescott, refnx: neutron and X-ray reflectometry analysis in Python, J. Appl. Cryst. 52 (2019) 193–200.

[72] D. Sivia, J. Webster, The Bayesian approach to reflectivity data, Phys. B 248 (1–4) (1998) 327–337.
[73] A. McCluskey, J. Cooper, T. Arnold, T. Snow, A general approach to maximise information density in neutron reflectometry analysis, Mach. Learn.: Sci. Technol. 1 (2020), 035002.
[74] F. Heinrich, P. Kienzle, D. Hoogerheide, M. Lösche, Information gain from isotopic contrast variation in neutron reflectometry on protein–membrane complex structures, J. Appl. Cryst. 53 (2020) 800–810.
[75] A. Gottwald, K. Wiese, U. Kroth, M. Richter, Uncertainty analysis for the determination of B4C optical constants by angle-dependent reflectance measurement for 40 nm to 80 nm wavelength, Appl. Opt. 56 (20) (2017) 5768–5774.
[76] A. Gottwald, K. Wiese, T. Siefke, M. Richter, Validation of thin film TiO2 optical constants by reflectometry and ellipsometry in the VUV spectral range, Meas. Sci. Technol. 30 (4) (2019), 045201.
[77] L.G. Parratt, Surface studies of solids by total reflection of X-rays, Phys. Rev. 95 (2) (1954) 359–369.
[78] L. Névot, P. Croce, Caractérisation des surfaces par réflexion rasante de rayons X. Application à l'étude du polissage de quelques verres silicates, Rev. Phys. Appl. 15 (3) (1980) 761–779.
[79] D. Foreman-Mackey, D. Hogg, D. Lang, J. Goodman, emcee: the MCMC hammer, Publ. Astron. Soc. Pac. 125 (925) (2013) 306–312.
[80] J. Goodman, J. Weare, Ensemble samplers with affine invariance, Commun. Appl. Math. Comput. Sci. 5 (1) (2010) 65–80.
[81] S. Heidenreich, H. Gross, M. Bar, Bayesian approach to the statistical inverse problem of scatterometry: comparison of three surrogate models, Int. J. Uncertain. Quan. 5 (6) (2015) 511–526.
[82] R. Bellman, Combinatorial processes and dynamic programming, RAND Corp. St. Monica (1958) 20.
[83] F. Kuo, I. Sloan, Lifting the curse of dimensionality, Not. AMS 52 (11) (2005) 1320–1328.
[84] R. Soufli, E. Gullikson, Reflectance measurements on clean surfaces for the determination of optical constants of silicon in the extreme ultraviolet–soft-x-ray region, Appl. Opt. 36 (22) (1997) 5499–5507.
[85] A. Andrle, P. Hönicke, J. Vinson, R. Quintanilh, Q. Saadeh, S. Heidenreich, F. Scholze, V. Soltwisch, The anisotropy in the optical constants of quartz crystals for soft X-rays, J. Appl. Crystallogr. 54 (2) (2021) 402–408.
[86] E. Falcao, F. Wudl, Carbon allotropes: beyond graphite and diamond, J. Chem. Technol. Biotechnol. 82 (2007) 524–531.
[87] D. Foreman-Mackey, corner.py: scatterplot matrices in python, J. Open Source Softw. 1 (2) (2016) 24.
[88] J. Hunter, Matplotlib: a 2D graphics environment, Com. Sci. Eng. 9 (3) (2007) 90–95.
[89] S. Valencia, A. Gaupp, W. Gudat, H.-Ch Mertins, P. Oppeneer, D. Abramsohn, C. Schneider, Faraday rotation spectra at shallow core levels: 3p edges of Fe, Co, and Ni, N. J. Phys. 8 (2006) 254.
[90] N. Brimhall, N. Herrick, D. Allred, R. Turley, M. Ware, J. Peatross, Measured optical constants of copper from 10 nm to 35 nm, Opt. Express 17 (26) (2009) 23873–23879.
[91] N. Brimhall, N. Herrick, D. Allred, R. Turley, M. Ware, J. Peatross, Characterization of optical constants for uranium from 10 to 47 nm, Appl. Opt. 49 (9) (2010) 1581–1585.
[92] R. Soufli, F. Delmotte, J. Meyer-Ilse, F. Salmassi, N. Brejnholt, S. Massahi, D. Girou, F. Christensen, E. Gullikson, Optical constants of magnetron sputtered Pt thin films with improved accuracy in the N- and O-electronic shell absorption regions, J. Appl. Phys. 125 (2019), 085106.
[93] N. Pauly, F. Yubero, S. Tougaard, Optical properties of molybdenum in the ultraviolet and extreme ultraviolet by reflection electron energy loss spectroscopy, Appl. Opt. 59 (2020) 4527–4532.
[94] R. Haensel, C. Kunz, T. Sasaki, B. Sonntag, Absorption measurements of copper, silver, tin, gold, and bismuth in the far ultraviolet, Appl. Opt. 7 (2) (1968) 301–306.
[95] R. Bruhn, B. Sonntag, H. Wolff, 3p excitations of atomic and metallic Fe, CO, Ni and Cu, J. Phys. B: At. Molec. Phys. 12 (2) (1979) 203–212.
[96] A. Asmussen, H. Riegler, Numerical analysis of x-ray reflectivity data from organic thin films at interfaces, J. Chem. Phys. 104 (20) (1996) 8159–8164.
[97] B. Sullivan, C. Montcalm, Extreme-ultraviolet optical constant determination near an absorption edge, Appl. Opt. 30 (28) (1991) 4010–4011.
[98] L. Smardz, U. Köbler, W. Zinn, Oxidation kinetics of thin and ultrathin cobalt films, J. Appl. Phys. 71 (10) (1992) 5199–5204.
[99] G. van Gurp, C. Langereis, Cobalt silicide layers on Si. I. Structure and growth, J. Appl. Phys. 46 (10) (1975) 4301–4307.
[100] B. Vodungbo, A. Sardinha, J. Gautier, G. Lambert, C. Valentin, M. Lozano, G. Iaquaniello, F. Delmotte, S. Sebban, J. Lüning, P. Zeitoun, Polarization control of high order harmonics in the EUV photon energy range, Opt. Express 19 (5) (2011) 4346–4356.
[101] D. Zusin, P. Tengdin, M. Gopalakrishnan, C. Gentry, A. Blonsky, M. Gerrity, D. Legut, J. Shaw, H. Nembach, T. Silva, P. Oppeneer, H. Kapteyn, M. Murnane, Direct measurement of the static and transient magneto-optical permittivity of cobalt across the entire M -edge in reflection geometry by use of polarization scanning, Phys. Rev. B 97 (2018), 024433.
[102] The periodictable Python package. Compiled by P. Kienzle with contributions from Distributed Data Analysis for Neutron Scattering Experiments (DANSE) project. Accessible via; < https://periodictable.readthedocs.io/en/latest/index.html >.
[103] S. Lam, A. Pitrou, S. Seibert, Numba: a LLVM-based python JIT compiler, Proc. Second Workshop LLVM Compil. Infrastruct. HPC (2015) 1–6.